metals

MDPI

Article

Transformation of Oxide Inclusions in Stainless Steel Containing Yttrium during Isothermal Heating at 1473 K

Xueliang Zhang [1,2], Shufeng Yang [1,3,*], Jingshe Li [1,*] and Jinqiang Wu [1]

[1] School of Metallurgical and Ecological Engineering, University of Science and Technology Beijing, Beijing 100083, China
[2] Department of Material Science and Engineering, Missouri University of Science and Technology, Rolla, MO 65409, USA
[3] Center for Innovation through Visualization and Simulation, Purdue University Northwest, Hammond, IN 46323, USA
* Correspondence: yangshufeng@ustb.edu.cn (S.Y.); lijingshe@ustb.edu.cn (J.L.); Tel.: +86-010-62334277 (S.Y.); +86-010-62334816 (J.L.)

Received: 17 July 2019; Accepted: 28 August 2019; Published: 1 September 2019

Abstract: To provide fundamental information on the control of rare earth inclusions in solid steel, two 18 mass% Cr-8 mass% Ni stainless steels with different yttrium additions were prepared using an electric resistance furnace and the evolution of yttrium-based oxide inclusions during heat treatment of the steels at 1473 K was investigated. In both as-cast steels, homogeneous spherical Al-Y-Si(-Mn-Cr) oxide inclusions were observed; however, the steel with larger yttrium additions also had some heterogeneous oxide inclusions with double phases. After heating, a new oxide phase with higher yttrium content precipitated from the original inclusions and resulted in partitioning to Y-rich and Al-rich parts in both steels. The average size and number density of inclusions slightly increased, and the morphology of inclusions changed from spherical to irregular. The transformation mechanism during isothermal heating was proposed to be the mutual effects of (*i*) internal transformation of the yttrium-based inclusions owing to crystallization of glassy oxide and (*ii*) interfacial reaction between inclusions and the steel matrix.

Keywords: non-metallic inclusions; stainless steel; yttrium addition; isothermal heating

1. Introduction

With the increasing demand for high-performance stainless steel, rare earth metals (REM), such as cerium, lanthanum, and yttrium, have been extensively applied in the steel manufacturing process. It has been reported that the addition of REM to stainless steel can significantly improve its corrosion resistance and mechanical properties such as strength, hot ductility, toughness, and oxidation resistance [1–5]. There are three main functions for REM in steel: modifying inclusions, deeply purifying molten steel, and alloying [6]. Among them, modifying inclusions is an extremely important one due to the close relationship between steel properties and the characteristics of inclusions in steel.

The influence of different REM on the behavior of inclusions at steelmaking temperature has been well investigated [7–12]. Dan et al. [7] studied the deoxidation characteristic of Al-Ce and Al-Y complex deoxidizers in molten iron. Compared with deoxidation of Al alone, lower deoxidation rates and higher oxygen content were observed after Al-Ce and Al-Y addition. The higher specific density of rare earth oxide inclusions compared to Al_2O_3 inclusions was considered to be the main reason for reducing the flotation of inclusions from the melt. With increasing cerium or yttrium content, the

morphology of inclusions changed from dendritic to globular. A similar result was also observed by Katsumata et al. in 25 mass% Cr-6 mass% Ni stainless steel [8]. Kwon et al. [9,10] investigated the evolution of inclusions in Al-killed stainless steel with Ce addition at 1873 K. Mn(Cr)-silicates were found to be the primary inclusions before Al addition. When Al was added without Ce addition, the initial Mn(Cr)-silicate changed to Al_2O_3-rich inclusions. Then, Al-Ce complex inclusions were formed in the steel after Ce addition due to the reaction between Ce and Al_2O_3 particles. Jönsson et al. [11,12] investigated the three-dimensional characteristics of clusters in REM-alloyed (Ce, La, Pr, and Nd) stainless steel through an electrolytic extraction method. It was found that most of the REM cluster consisted of regular and irregular REM-oxides, and the size of these clusters varied in the range of 2 to 23 μm. Moreover, turbulent collisions were determined to be the dominant form for the growth of REM clusters. With increasing the size of clusters, the growth rate of REM clusters increased.

The changing behavior of rare earth inclusions in molten steel is relatively clear now; however, less attention has been paid to the possible transformation of rare earth inclusions in solid steel during heat treatment. This is practically important because steel quality significantly depends on the final state of inclusions after different thermal and mechanical treatments [13]. Many researchers have reported that some inclusions would change during heat treatment [14–21]. In 18 mass% Cr-8 mass% Ni austenitic stainless steel, MnO-SiO_2 oxide inclusions changed to finer MnO-Cr_2O_3 spinel during heat treatment at 1473 K due to the interfacial reaction between inclusions and steel matrix [14–18]. Grain growth during heat treatment was also suppressed effectively by the newly formed small MnO-Cr_2O_3 particles because of the pinning effect [15]. The evolution of Al-Ti oxide inclusions in Fe-Al-Ti alloy during heat treatment was also investigated through laboratory experiments [19–23]. Homogeneous Al-Ti oxide inclusions were observed in as-cast alloys, while most of the homogeneous oxide inclusions transformed into heterogeneous ones with Al-rich and Ti-rich parts after heat treatment at 1573 K. The shape of the oxide inclusions also changed from spherical to irregular. The transformation mechanism of the Al-Ti oxide inclusions was proposed as the precipitation of Al_2O_3 from the initial inclusions due to the crystallization of glassy oxide during heating. Furthermore, the evolution of MnS inclusions during heat treatment of E36 shipbuilding steel with Mg addition at 1473 K was also investigated by Wang et al. [22,23]. It was found that the individual MnS inclusions in cast billet changed to MnS- and Al-Mg-Ti oxide- combined type inclusions after heating. Also, this change significantly promoted the formation of acicular ferrites in steel.

Yttrium, as a reactive element, has not only some similarities with cerium and laudanum but also exhibits its own unique features. Recently, adding yttrium to steels has been considered due to its effects of deoxidizing, desulfurizing, and refining as-cast microstructure [24–26]. Stainless steel processing typically includes heating before hot rolling, so it is essential to understand the possible transformation of non-metallic inclusions during the whole industrial process. However, to the authors' best knowledge, there is little literature focusing on the changing behavior of yttrium-based oxide inclusions during heat treatment. Therefore, in the present study, the evolution of oxide inclusions in Y-added stainless steel during isothermal heating at 1473 K was investigated for a better understanding of the control of non-metallic inclusions and the application of yttrium metal in steel.

2. Materials and Methods

2.1. Preparation of Stainless Steel

Two steels referred to as #1 and #2 with different yttrium contents were prepared by the following procedure: A 180 g specimen from as-received 304 stainless steel was melted in an Al_2O_3 crucible (diameter: 35 mm, height: 70 mm) and placed in a Si-Mo electric resistance furnace under high-purity argon gas (>99.999%, flow rate: 0.3 m^3/h). After melting at 1873 K for 15 min, 0.02 g or 0.06 g Fe-65 mass% Y alloy wrapped by pure iron foil was added into the melt by a molybdenum rod, followed by stirring for 10 s to guarantee uniform composition of the molten steel. After 10 min of holding, the crucible was taken out and quenched by ice water. Chemical composition of Mn, Si, Al, and Y was

determined by inductively coupled plasma optical emission spectrometry (ICP-OES) and total oxygen content (T.O.) was determined by inert gas fusion. Table 1 shows the composition of the Y-added stainless steels.

Table 1. Chemical composition of the steels (mass%).

Steel	Fe	Cr	Ni	Si	Mn	Al_t	Y	T.O
#1	Bal.	18	8	0.38	1.55	0.006	0.0085	0.011
#2	Bal.	18	8	0.38	1.55	0.010	0.0180	0.014

2.2. Isothermal Heating

Several cylindrical samples (diameter: 8 mm, height: 15 mm) were machined from each quenched steel and divided into two groups: as-cast and heat-treated. In order to study the evolution of non-metallic inclusions during heat treatment, the samples were heated in a horizontal electric resistance furnace for 0.5, 1, and 2 h at 1473 K, respectively. A Pt 30% Rh-Pt 6% Rh thermocouple was employed to determine the constant temperature zone of the heating furnace. The temperature deviation was controlled in the range of ±5 K during heat treatment, and high purity argon gas (>99.999%, flow rate: 0.2 m^3/h) was introduced to prevent oxidation of samples. After heating, the samples were taken out quickly and quenched by water.

2.3. Inclusion Characterization

The quenched as-cast and heat-treated samples were machined to expose the vertical section, and then ground by SiC paper and polished by diamond suspensions up to 0.1 μm. A scanning electron microscope equipped with energy-dispersive spectrometry (SEM-EDS, Phenom ProX, Holland) was used to characterize the non-metallic inclusions. At least 50 inclusions were characterized for each sample. In addition, about 40 to 45 optical images were taken from each steel sample under ×1500 magnification, and the size distribution of inclusions was analyzed in 0.96 mm^2 by Image Pro-Plus 6.0 Software.

3. Results

3.1. Characterization of Inclusions in the As-Cast Steels

In this study, the atomic concentrations of Y, Al, Si, Mn, Cr, and O in inclusions were determined by energy-dispersive spectrometry (EDS). Based on the conservation of atoms, the molar fraction of each component in the Y_2O_3-Al_2O_3-SiO_2-MnO-Cr_2O_3 system was calculated. Figure 1 shows the morphology and composition of typical inclusions in as-cast steels. Homogeneous oxide inclusions consisting of $34Al_2O_3$-$27SiO_2$-$19Y_2O_3$-14MnO-$7Cr_2O_3$ (mol%) were observed in as-cast steel #1. The composition distribution of inclusions was plotted on the Y_2O_3-Al_2O_3-(SiO_2 + MnO + Cr_2O_3) ternary diagram, as shown in Figure 2a. Two kinds of oxide inclusions were found in as-cast steel #2 treated by higher yttrium addition: heterogeneous inclusions with two phases (black phase and white phase) and homogeneous ones. As illustrated in Figure 2b, the composition of the black phase in heterogeneous inclusions was similar to that of the homogeneous ones in steel #2, while higher Y_2O_3 content was detected in the white phase of the heterogeneous inclusions. In both as-cast steels, #1 and #2, the oxide inclusions were spherical, indicating the formation of a liquid phase at steelmaking temperature.

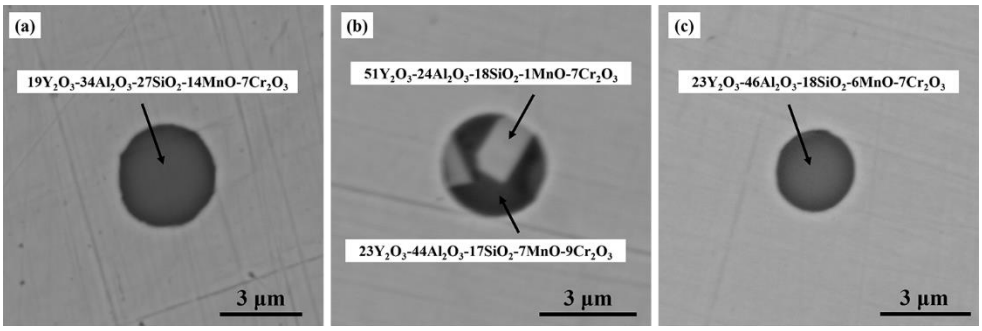

Figure 1. Typical inclusions in as-cast steel #1 (**a**) and #2 (**b**,**c**).

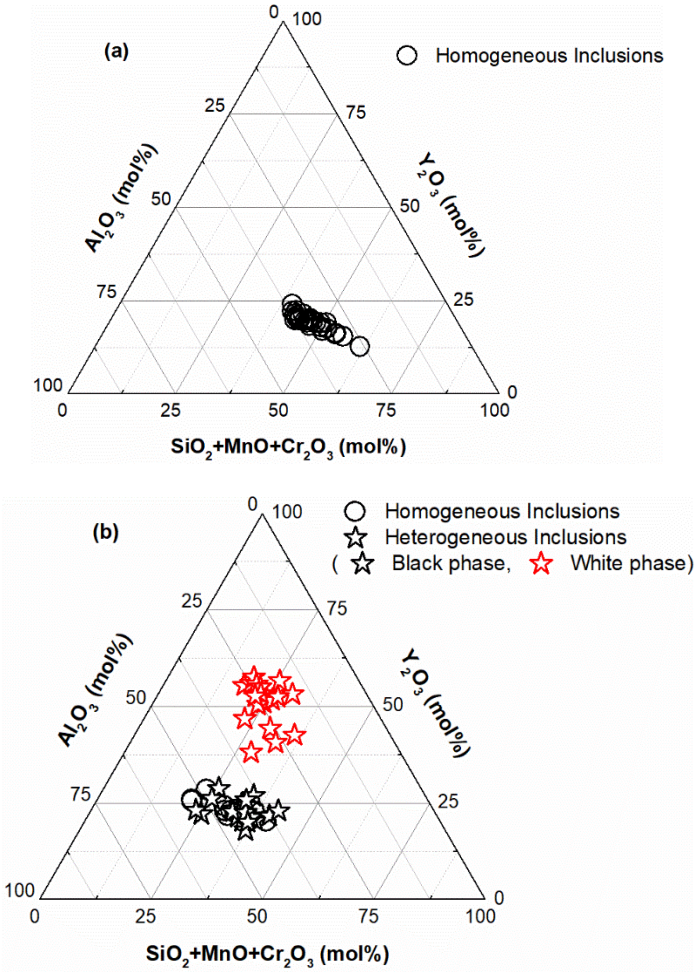

Figure 2. Composition distribution of oxide inclusions in as-cast steel #1 (**a**) and #2 (**b**).

The size distribution of inclusions in steel #1 and #2 is presented in Figure 3. Similar trends were observed in both steels. Most of the oxide inclusions were smaller than 3 μm, and the fractions of the inclusions with 1.0–1.5 μm and 1.5–2.0 μm diameters were approximately 60% and 25%, respectively. The same results were also found in the studies of cerium-treated stainless steel [7,8], indicating that fine inclusions are easier to form in REM-treated melt.

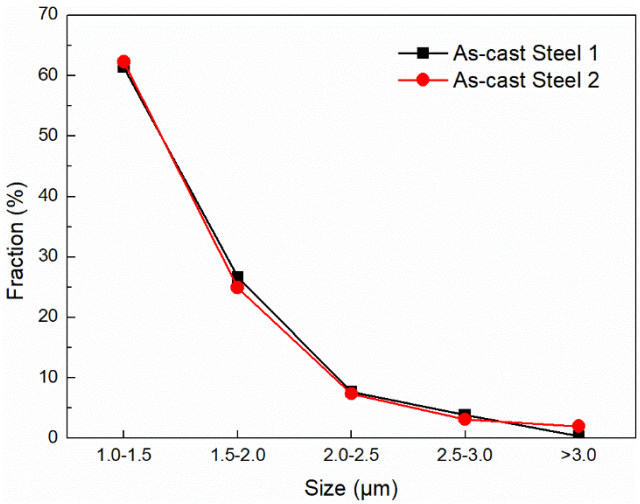

Figure 3. Size distribution of inclusions in as-cast steels.

3.2. Transformation of Oxide Inclusions during Isothermal Heating

Figure 4 shows the morphology of typical oxide inclusions in steel #1 after isothermal heating at 1473 K. It was found that the homogeneous oxide inclusions changed to heterogeneous ones after heat treatment. Instead of the oxide inclusions with a single black phase, a new gray phase with higher Y_2O_3 content precipitated on the inclusions. The shape of inclusions also changed from spherical to irregular.

A similar transformation was observed in steel #2 (see Figure 5). The change in the original heterogeneous inclusions is shown in Figure 5a–c. The white phase in the inclusions looked stable during heating, while the black phase was partially substituted by a newly-precipitated gray phase, and the shape of inclusions changed to irregular. Figure 5d–f shows the transformation of homogeneous inclusions in steel #2. Most of the part of the black phase in the oxide inclusions changed to a gray phase after heating, and only a small amount of black phase was left on the edge of the inclusions. With increasing heating time from 0.5 to 2 h, more oxide inclusions containing white phase were found, which may indicate that part of the newly formed gray phase changed to the white phase during heating.

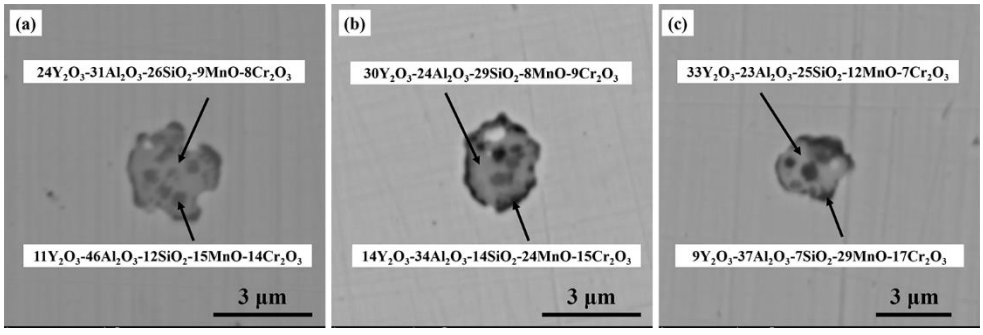

Figure 4. Morphology of typical oxide inclusions in steel #1 after isothermal heating for 0.5 h (**a**), 1.0 h (**b**), and 2.0 h (**c**).

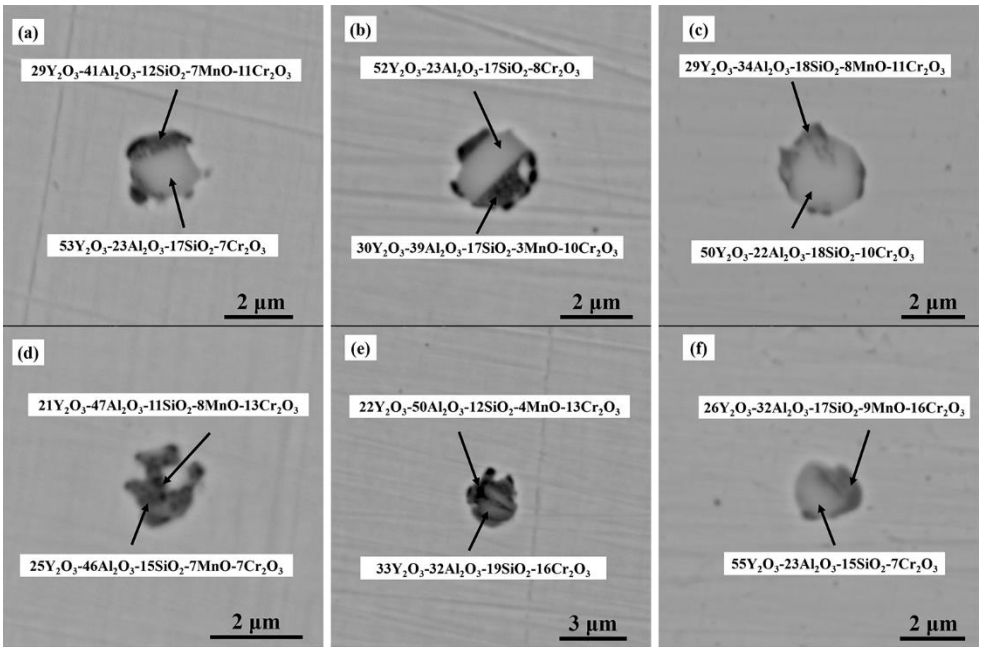

Figure 5. Morphology of typical oxide inclusions in steel #2 after isothermal heating for 0.5 h (**a**) and (**d**), 1.0 h (**b**) and (**e**), and 2.0 h (**c**) and (**f**).

In order to get more detailed information about the heterogeneous inclusions formed during heat treatment, mapping analysis of the typical oxide inclusion in heated steels was done, as illustrated in Figure 6. It can be seen that the gray part of the oxide inclusion corresponded to the Y-rich phase and the black area depicted the Al-rich phase. The heterogeneous oxide inclusion in heated steels was also analyzed by a scanning line, as seen in Figure 7. It is worth noting that the Al, Y, and O concentration gradients existed within the Y-rich part of the inclusion with a width of approximately 1.2 μm observed.

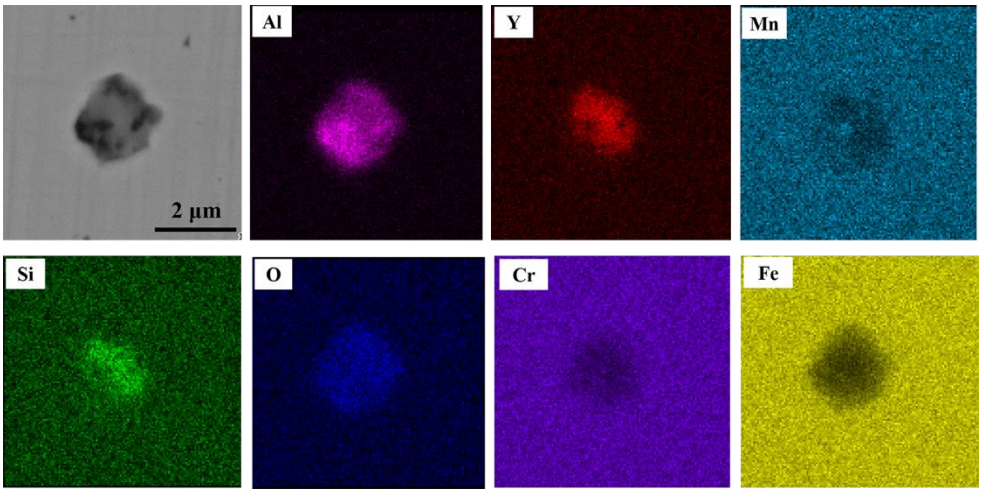

Figure 6. Mapping analysis of typical oxide inclusions after heating.

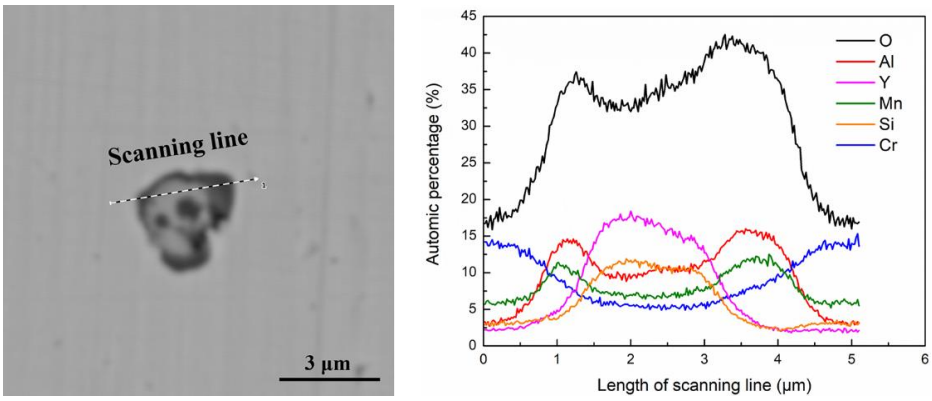

Figure 7. Scanning line analysis of the heterogeneous oxide inclusion.

As mentioned above, the composition of the oxide inclusions changed after heating at 1473 K. Figure 8 shows the change in the composition of inclusions from as-cast condition compared to after heating for 2 h. In heated steel #1 (Figure 8a), Y_2O_3 content in the gray phase of inclusions became higher compared to that in as-cast condition, and the Y/Al ratio increased from 0.56 to 1.37, while the Y_2O_3 content in the residual black phase was reduced, and the Y/Al ratio decreased to 0.26.

In heated steel #2 (Figure 8b), there was no noticeable change in the composition of the white phase in heterogeneous inclusions after heating for 2 h, while similar transformation to that found in steel #1 was also observed for the initially homogeneous inclusions (black phase). The Y/Al ratio of inclusions increased from 0.53 to 0.93, causing the transformation of the black phase to the gray phase. Meanwhile, a little residual black phase with a lower Y/Al ratio was also observed.

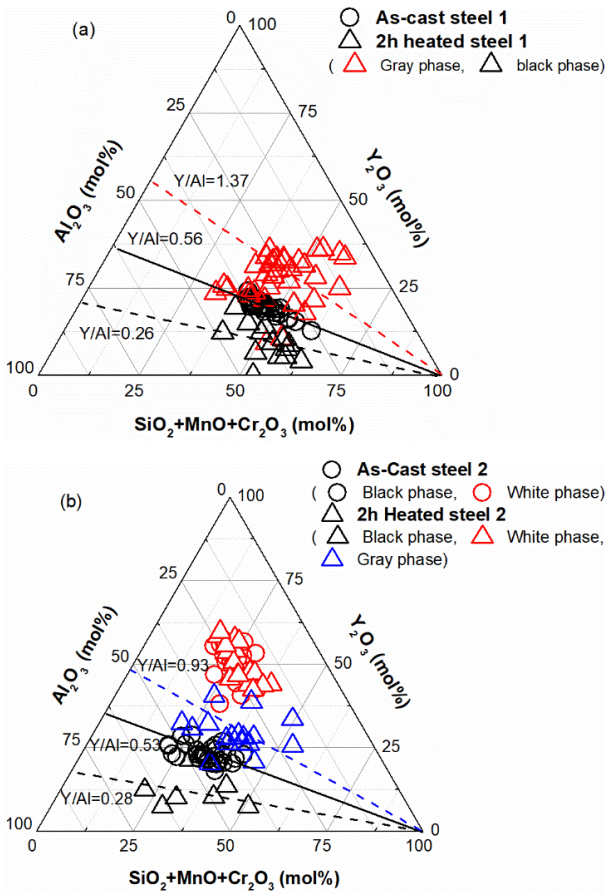

Figure 8. Composition distributions of oxide inclusions in steel #1 (**a**) and #2 (**b**) after heating for 2 h.

Figure 9 shows the variation of the composition of oxide inclusions in steel #1 with heating time. The Y_2O_3 content in the oxide inclusions increased from 18% to 25% and the Al_2O_3 content decreased from 34% to 26% after heating for 0.5 h (see Figure 9a), which resulted in the formation of a new gray phase (Y-rich part) in inclusions. With increasing heating time, the contents of Y_2O_3 and Al_2O_3 in the gray phase gradually increased and decreased, respectively. However, the contents of SiO_2, MnO, and Cr_2O_3 in the gray phase did not obviously change during heating.

The composition of the residual black phase (Al-rich part) in oxide inclusions was also analyzed after heating (see Figure 9b). The Y_2O_3 content in the black phase was reduced from 18% to 10% after heating for 0.5 h. The Al_2O_3 content slightly increased from 34% to approximately 39%. In addition, due to the interfacial reaction between oxide inclusions and steel matrix during heating [16,17], a distinct change in the contents of SiO_2, MnO, and Cr_2O_3 was also observed: SiO_2 content decreased from 28% to 12% and MnO and Cr_2O_3 contents increased from 9% and 6% to 30% and 15%, respectively. With increasing heating time from 0.5 to 2 h, there was no significant change in the composition of the black phase inclusions.

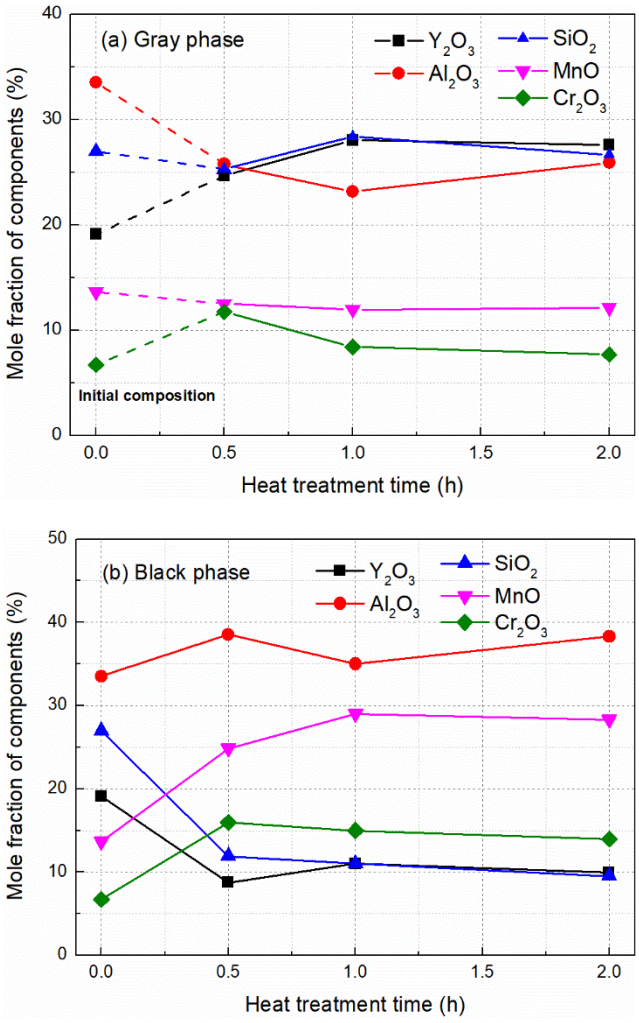

Figure 9. Change in composition of oxide inclusions in steel #1 during heating: gray phase (**a**) and black phase (**b**).

Figure 10 shows the change in the composition of oxide inclusions in steel #2 during heating. In as-cast condition, this steel had two types of inclusions: homogeneous (black phase) and heterogeneous with the Y-rich white phase, as illustrated in Figure 1b,c. During heating, the part of the homogeneous black phase in inclusions was changed to two phases: residual black phase (Al-rich

part) and gray phase (Y-rich part). The amount of Al_2O_3 component in the gray phase was depleted during the heat treatment and then the Y-rich part was formed. This transformation was similar to that observed in steel #1. The contents of Al_2O_3 and Y_2O_3 in the newly formed gray phase decreased and increased, respectively, after heating (Figure 10a). During this depletion, the Al_2O_3 content in the residual black phase slightly increased, but the Y_2O_3 content decreased (Figure 10b). However, it was found that the composition of the white phase originally presented in heterogeneous particles didn't change during heating (Figure 10c).

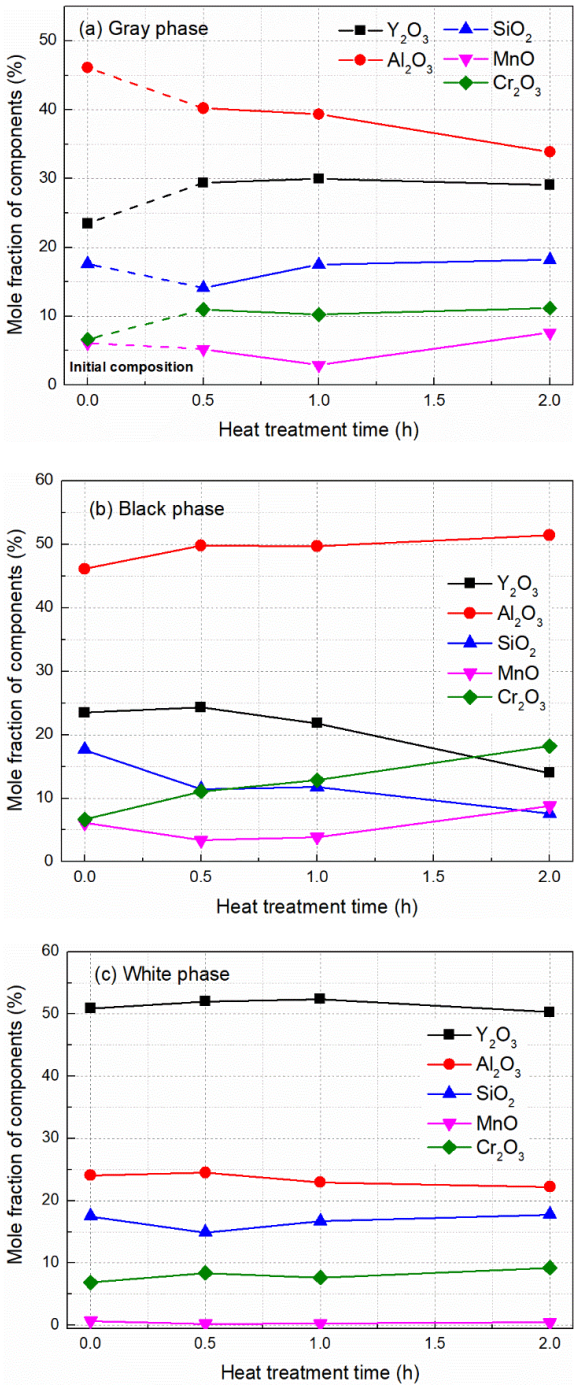

Figure 10. Change in composition of oxide inclusions in steel #2 during heating. gray phase (**a**), black phase (**b**), and white phase (**c**).

The fraction of inclusion families containing different phases in steel #2 is shown in Figure 11. The fraction of inclusions containing the black phase was significantly reduced from 100% to 20% after heating, owing to the change of as-cast oxide inclusions from the black phase to the gray phase. The fraction of inclusions containing the gray phase first increased to 98%, then slightly decreased. However inclusions containing the white phase, gradually increased from 70% to 90% during heating, which may indicate that the transformation of inclusions from the gray phase to the white phase happened.

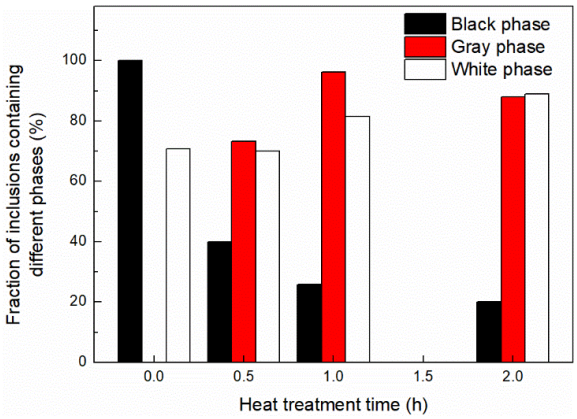

Figure 11. Fraction of inclusions containing different phases in steel #2 after heating.

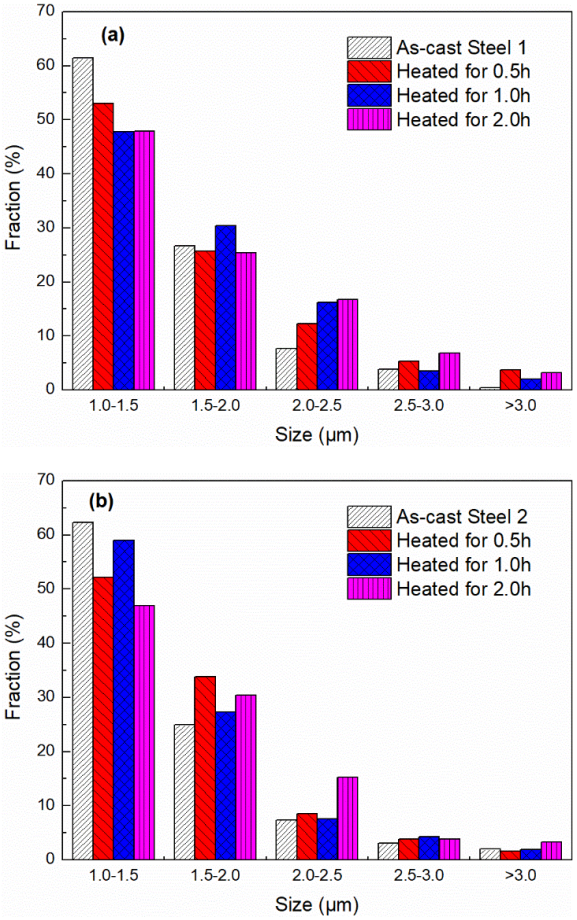

Figure 12. Size distribution of oxide inclusions after heating in steel #1 (**a**) and #2 (**b**).

Figure 12 illustrates the size distribution of inclusions in steels #1 and #2 after heating. The size of most oxide inclusions was still less than 3 μm. Compared with the size distribution of inclusions in

as-cast steels, the fraction of inclusions with 1.0–1.5 μm diameter was reduced from 60% to about 50% after heating, while the fraction of inclusions with larger size (≥2.0 μm in steel #1, and ≥1.5 μm in steel #2) slightly increased.

Figure 13 shows the change in the average size and number density of inclusions during heating. At least one hundred inclusions were analyzed in each sample, and the maximum diameter of inclusion was used to represent the size of one particle. During heating, the average size of oxide inclusions in both steels increased from 1.5 to 1.7 μm. The number density of inclusions in both steels #1 and #2 also slightly increased from 278/mm^2 and 367/mm^2 to 289/mm^2 and 416/mm^2, respectively, after heating for 2 h. By comparing the number density of inclusions in steels #1 and #2, it was easy to find that there were more inclusions in steel #2, which indicated more rare earth oxide inclusions formed in the steel with higher yttrium addition.

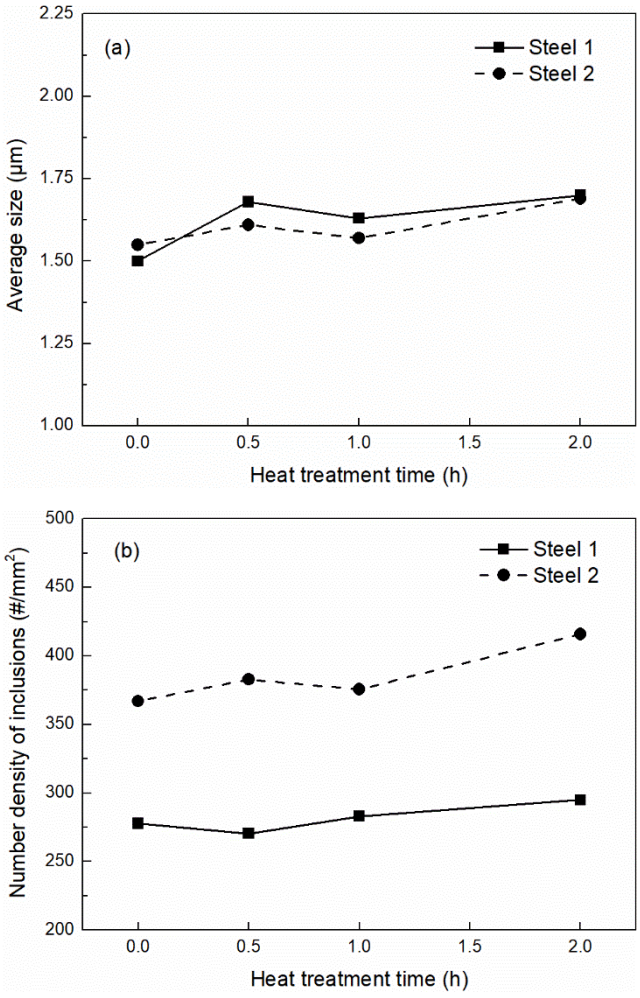

Figure 13. Change in average size (**a**) and number density (**b**) of oxide inclusions during heating at 1473 K.

4. Discussion

Due to the high cooling rate, the inclusions in as-cast specimens can be considered as the same as those in molten steel. As shown in Figure 1, homogeneous spherical Al-Y-Si(-Mn-Cr) oxide inclusions were observed in both as-cast steels. At the same time, some heterogeneous globular oxide inclusions with Y-rich phase were also found in as-cast steel #2 owing to the more substantial yttrium addition. The inclusions in the two as-cast specimens were fine, and the size of most inclusions were smaller than 3 μm. After isothermal heating at 1473 K, a gray phase with higher yttrium content precipitated from the original inclusions in both steels #1 and #2, resulting in the separation of inclusions to Y-rich and

Al-rich parts as illustrated in Figure 4. Moreover, the shape of inclusions also changed from spherical to irregular. The comparison of the size distribution of inclusions in as-cast and heated steels showed that more inclusions with larger size were present after heating (see Figure 12), and the number density of inclusions also slightly increased (see Figure 13). This may indicate an increase in the total volume of inclusions in steel after heat treatment.

Based on the experimental results mentioned above, the transformation mechanisms of the yttrium-based oxide inclusions during heat treatment were proposed to be mutual effects of *(i)* internal transformation of inclusions and *(ii)* interfacial reaction between inclusions and steel matrix.

4.1. Internal Transformation of Inclusions

Many studies on the phase equilibrium, phase separation, and crystallization behavior of the Al_2O_3-Y_2O_3-SiO_2 system under long heat-treatment conditions (from room temperature to 1350 °C) have been reported [27–32]. The phase separation as an early stage of crystallization was observed during heat treatment of the glassy system [27] and the two phases of Y_2O_3-SiO_2 and Al_2O_3-SiO_2 precipitated from the Al_2O_3-Y_2O_3-SiO_2 system due to the diffusion of Al^{3+} and O^{2-} during heat treatment [29,32].

Therefore, in this study, the transformation of yttrium-based oxide during heating at 1473 K was supposed to involve the internal transformation of inclusions caused by the crystallization of the oxide from glassy state. The schematic of the transformation mechanism of yttrium-based oxide inclusions is shown in Figure 14. During heat treatment at 1473 K, the Al^{3+} and O^{2-} in the Al-Y-Si(-Mn-Cr) oxide diffused from the inside to the surface of the inclusion and precipitated through heterogeneous nucleation, resulting in the formation of an Al-rich part (black phase) around the inclusion and the precipitation of a Y-rich part (gray phase) in the core of the inclusion (see Figure 5). Therefore, Al and O concentration gradients were observed in the Y-rich part of the oxide particle, as seen in Figure 7.

There are three kinds of compounds for yttrium aluminum double oxides: $Y_3Al_5O_{12}$ (yttrium aluminum garnet, YAG), $YAlO_3$ (yttrium aluminum perovskite, YAP), and $Y_4Al_2O_9$ (yttrium aluminum monoclinic, YAM) [33,34]. As illustrated in Figure 8, the Y/Al ratio of the inclusions changed from 0.6 to around 1.0 (Y-rich part, gray phase) and 0.3 (Al-rich part, black phase) after heating. It is speculated that the yttrium-based oxide inclusions probably transformed from the $Y_3Al_5O_{12}$-SiO_2 system to $YAlO_3$-SiO_2 (close to the Y-rich part) and Al_2O_3-SiO_2 (close to the Al-rich part) during heating at 1473 K.

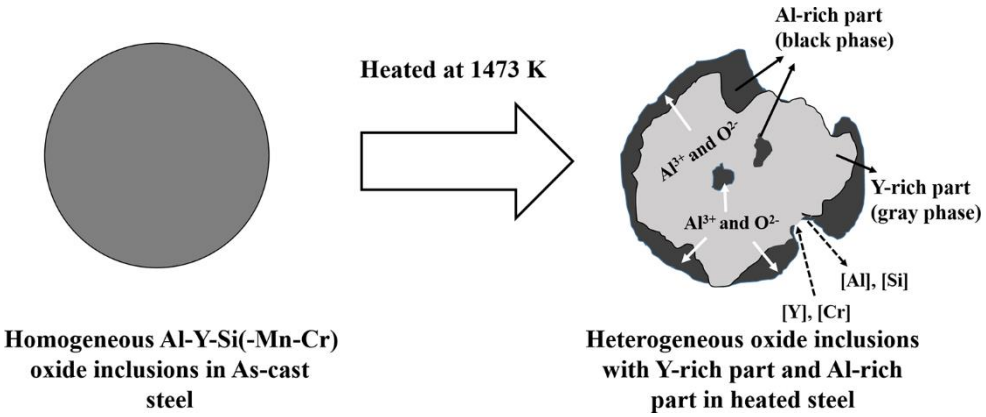

Figure 14. Schematic of the transformation mechanism of yttrium-based oxide inclusions during isothermal heating at 1473 K.

4.2. Interfacial Reaction between Inclusions and Steel Matrix

Solid-state interfacial reaction between some oxide inclusions and steel matrix could occur during heat treatment. This has been confirmed in 18 mass% Cr-8 mass% Ni stainless steel [14–18]. In this study, the same transformation was also observed in both steels #1 and #2. As shown in Figures

9b and 10b, decrease in SiO_2 content and increase in Cr_2O_3 content in inclusions were detected in the residual black phase of inclusions after heating. An interfacial reaction between the oxide inclusions and chromium element in steel matrix was considered to have happened and resulted in the transformation of MnO-SiO_2 type to MnO-Cr_2O_3 type.

Yttrium, as a reactive element, has stronger thermodynamic affinity with oxygen than Al element does [35,36]. With decreasing temperature, the solubility of yttrium in steel matrix would decrease [37]. Therefore, it is possible that the yttrium element in solid steel diffused to the surface of inclusions and an interfacial reaction occurred during heating, as illustrated in Figure 14. The possible reaction is shown in equation (1). However, due to the lack of thermodynamic data of the Y-Al-Fe-O system at 1473 K, the related data in liquid iron were assumed to be applicable at this temperature, as presented in Equation (2) [38,39]. The thermodynamic calculations were done based on the following assumptions: (1) the activity coefficient of Y and Al in liquid iron was unity due to their low contents and (2) Y_2O_3 and Al_2O_3 were considered to be pure substances.

$$2[Y]_{(\text{solid steel})} + Al_2O_{3(\text{inclusion})} = Y_2O_{3(\text{inclusion})} + 2[Al]_{(\text{solid steel})} \quad (1)$$

$$2[Y] + Al_2O_3(s) = Y_2O_3(s) + 2[Al] \quad (2)$$

$$\Delta G^\circ = -565{,}768+268T \text{ (J/mol)} \quad (3)$$

The Gibbs energy changes of this reaction at 1473 K were −179,535 J/mol and −185,400 J/mol in steels #1 and #2, respectively. These indicated that the interfacial reaction between yttrium-based oxide inclusions and steel matrix could occur during holding at 1473 K. An interfacial reaction product layer would form on the surface of inclusions during heating, and it could cause an increase in the size of inclusions. As shown in Figure 12, more inclusions with larger size were found in both steels after heating, which was consistent with the theoretical analysis.

5. Conclusions

The evolution of rare earth oxide inclusions during isothermal heating at 1473 K was investigated in two stainless steels with different yttrium contents. The following conclusions were made.

1. Yttrium-based oxide inclusions in both as-cast steels were characterized. Before heating, all the inclusions were spherical, and the size of them was less than 3 μm. Homogeneous Al-Y-Si(-Mn-Cr) oxide inclusions were observed in both as-cast steels. Meanwhile, some heterogeneous inclusions with double phases were also found in steel #2 with more yttrium addition.
2. After heat treatment, a gray phase with higher Y_2O_3 content precipitated from the original oxide inclusions, and all the inclusions transformed to heterogeneous ones with Y-rich (gray phase) and Al-rich (black phase) parts in both heated steels. The average size and number density of inclusions increased slightly, and the shape of inclusions changed from spherical to irregular.
3. The transformation mechanism of yttrium-based oxide inclusions during isothermal heating was proposed to be the mutual effects of *(i)* internal transformation of oxide inclusions owing to the crystallization of glassy oxide and *(ii)* interfacial reaction between the inclusions and steel matrix.

Author Contributions: Conceptualization, S.Y. and J.L.; Formal Analysis, X.Z.; Investigation, X.Z. and J.W.; Writing—Original Draft Preparation, X.Z.; Writing—Review and Editing, S.Y. and J.L.; Supervision, S.Y. and J.L.

Funding: This research was funded by National Natural Science Foundation of China (Grant Nos. 51674023, 51574190 and 51734003).

Acknowledgments: The China Scholarship Council (201806460049) is acknowledged. The authors would also like to thank Simon N. Lekakh at Missouri University of Science and Technology for his guidance on this work.

Conflicts of Interest: The authors declare no conflict of interest.

References

1. Samanta, S.; Mitra, S.; Pal, T. Effect of rare earth elements on microstructure and oxidation behaviour in TIG weldments of AISI 316L stainless steel. *Mater. Sci. Eng. A* **2006**, *430*, 242–247. [CrossRef]
2. Kim, S.; Jeon, S.; Lee, I.; Park, Y. Effects of rare earth metals addition on the resistance to pitting corrosion of super duplex stainless steel–Part 1. *Corros. Sci.* **2010**, *52*, 1897–1904. [CrossRef]
3. Chen, L.; Ma, X.; Wang, L.; Ye, X. Effect of rare earth element yttrium addition on microstructures and properties of a 21Cr-11Ni austenitic heat-resistant stainless steel. *Mater. Des.* **2011**, *32*, 2206–2212. [CrossRef]
4. Li, Y.; Liu, C.; Zhang, T.; Jiang, M.; Peng, C. Liquid inclusions in heat-resistant steel containing rare earth elements. *Mater. Trans. B* **2017**, *48*, 956–965. [CrossRef]
5. Jeon, S.; Kim, S.; Choi, M.; Kim, J.; Kim, K.; Park, Y. Effects of cerium on the compositional variations in and around inclusions and the initiation and propagation of pitting corrosion in hyperduplex stainless steels. *Corros. Sci.* **2013**, *75*, 367–375. [CrossRef]
6. Huang, Y.; Cheng, G.; Li, S.; Dai, W. Effect of Cerium on the Behavior of Inclusions in H13 Steel. *Steel Res. Int.* **2018**, *89*, 1800371. [CrossRef]
7. Dan, T.; Gunji, K. Deoxidation Characteristics and Shape Modification of Deoxidation Products with Al-Ce and Al-Y Complex Deoxidizers. *Tetsu-to-Hagané* **1982**, *68*, 1915–1921. [CrossRef]
8. Katsumata, A.; Todoroki, H. Effect of rare earth metal on inclusion composition in molten stainless steel. *Iron Steelmak.* **2002**, *29*, 51–57.
9. Kwon, S.; Kong, Y.; Park, J. Effect of Al deoxidation on the formation behavior of inclusions in Ce-added stainless steel melts. *Met. Mater. Int.* **2014**, *20*, 959–966. [CrossRef]
10. Kwon, S.; Park, J.; Park, J. Influence of refractory-steel interfacial reaction on the formation behavior of inclusions in Ce-containing stainless steel. *ISIJ Int.* **2015**, *55*, 2589–2596. [CrossRef]
11. Bi, Y.; Karasev, A.; Jönsson, P. Three dimensional evaluations of REM clusters in stainless steel. *ISIJ Int.* **2014**, *54*, 1266–1273. [CrossRef]
12. Nabeel, M.; Karasev, A.; Jönsson, P. Formation and Growth Mechanism of Clusters in Liquid REM-alloyed Stainless Steels. *ISIJ Int.* **2015**, *55*, 2358–2364. [CrossRef]
13. Kitamura, S. Preface to the Special Issue on Fundamentals and Applications of Non-metallic Inclusions in Solid Steel. *ISIJ Int.* **2011**, *51*, 1943. [CrossRef]
14. Takahashi, I.; Sakae, T.; Yoshida, T. Changes of the Nonmetallic Inclusion by Heating. *Tetsu-to-Hagané* **1967**, *53*, 168–173.
15. Takano, K.; Nakao, R.; Fukumoto, S.; Tsuchiyama, T.; Takaki, S. Grain size control by oxide dispersion in austenitic stainless steel. *Tetsu-to-Hagané* **2003**, *89*, 616–622. [CrossRef]
16. Shibata, H.; Tananka, T.; Kimura, K.; Kimura, S. Composition change in oxide inclusions of stainless steel by heat treatment. *Ironmak. Steelmak.* **2010**, *37*, 522–528. [CrossRef]
17. Shibata, H.; Kimura, K.; Tanaka, T.; Kitamura, S. Mechanism of change in chemical composition of oxide inclusions in Fe-Cr Alloys deoxidized with Mn and Si by heat treatment at 1473 K. *ISIJ Int.* **2011**, *51*, 1944–1950. [CrossRef]
18. Ren, Y.; Zhang, L.; Pistorius, P. Transformation of Oxide Inclusions in Type 304 Stainless Steels during Heat Treatment. *Metall. Mater. Trans. B* **2017**, *48*, 2281–2292. [CrossRef]
19. Choi, W.; Matsuura, H.; Tsukihashi, F. Changing behavior of non-metallic inclusions in solid iron deoxidized by Al–Ti addition during heating at 1473 K. *ISIJ Int.* **2011**, *51*, 1951–1956. [CrossRef]
20. Li, M.; Matsuura, H.; Tsukihashi, F. Evolution of Al-Ti Oxide Inclusion during Isothermal Heating of Fe-Al-Ti Alloy at 1573 K (1300 °C). *Mater. Trans. B* **2017**, *48*, 1915–1923. [CrossRef]
21. Li, M.; Matsuura, H.; Tsukihashi, F. Time-Dependent Evolution of Ti-Bearing Oxide Inclusions during Isothermal Holding at 1573 K (1300 °C). *Metall. Mater. Trans. A* **2019**, *50*, 863–873. [CrossRef]
22. Wang, Q.; Zou, X.; Matsuura, H.; Wang, C. Evolution of Inclusions During 1473 K Heating Process in EH36 Shipbuilding Steel with Mg Addition. *JOM* **2018**, *70*, 521–526. [CrossRef]
23. Zou, X.; Zhao, D.; Sun, J.; Wang, C.; Matsuura, H. An integrated study on the evolution of inclusions in EH36 shipbuilding steel with Mg addition: From casting to welding. *Metall. Mater. Trans. B* **2018**, *49*, 481–489. [CrossRef]

24. Fujikawa, H.; Morimoto, T.; Nishiyama, Y.; Newcomb, S. The effects of small additions of yttrium on the high-temperature oxidation resistance of a Si-containing austenitic stainless steel. *Oxid. Met.* **2003**, *59*, 23–40. [CrossRef]
25. Jiang, Q.; Liang, H.; Sui, H. Effect of Y-Ce complex modification on thermal fatigue behavior of high Cr cast hot working die steels. *ISIJ Int.* **2004**, *44*, 1762–1766. [CrossRef]
26. Yan, J.; Gao, Y.; Liang, L.; Ye, Z.; Li, Y.; Chen, W.; Zhang, J. Effect of yttrium on the cyclic oxidation behaviour of HP40 heat-resistant steel at 1373 K. *Corros. Sci.* **2011**, *53*, 329–337. [CrossRef]
27. Murakami, Y.; Yamamoto, H. Phase Equilibria in Al_2O_3-Y_2O_3-SiO_2 System and Phase Separation and Crystallization Behavior of Glass. *J. Ceram. Soc. Jpn.* **1991**, *99*, 215–221. [CrossRef]
28. Ahmad, S.; Ludwig, T.; Herrmann, M.; Mahmoud, M.; Lippmann, W.; Seifert, H. Phase evaluation during high temperature long heat treatments in the Y_2O_3-Al_2O_3-SiO_2 system. *J. Eur. Ceram. Soc.* **2014**, *34*, 3835–3840. [CrossRef]
29. Ahmad, S.; Herrmann, M.; Mahmoud, M.; Leiste, H.; Lippmann, W.; Seifert, H. Crystallisation studies of RE_2O_3-Al_2O_3-SiO_2 glasses under long heat-treatment conditions. *J. Alloys Compd.* **2016**, *688*, 762–774. [CrossRef]
30. Kolitsch, U.; Seifert, H.; Ludwig, T.; Aldinger, F. Phase equilibria and crystal chemistry in the Y_2O_3-Al_2O_3-SiO_2 system. *J. Mater. Res.* **1999**, *14*, 447–455. [CrossRef]
31. Almeida, J.; Fonseca, A.; Correia, R.; Baptista, J. Pressureless sintering of silicon nitride with additives of the Y_2O_3-Al_2O_3-SiO_2 system. *Mater. Sci. Eng. A* **1989**, *109*, 395–400. [CrossRef]
32. Wisniewski, W.; Keshavarzi, A.; Zscheckel, T.; Russel, C. EBSD-based phase identification in glass-ceramics of the Y_2O_3-Al_2O_3-SiO_2 system containing α-and β-$Y_2Si_2O_7$. *J. Alloys Compd.* **2017**, *699*, 832–840. [CrossRef]
33. Harada, M.; Goto, M. Synthesis of Y-Al-O compounds by a polymer complex method. *J. Alloys Compd.* **2006**, *408*, 1193–1195. [CrossRef]
34. Shen, Y.; Zou, T.; Zhang, S.; Sheng, L. Identification of oxide phases in oxide dispersion strengthened PM2000 steel. *ISIJ Int.* **2013**, *53*, 304–310. [CrossRef]
35. Han, Q.; Xiang, C.; Dong, Y.; Yang, S.; Chen, D. Equilibria between the rare earth elements, oxygen and sulfur, in molten iron. *Metall. Trans. B* **1988**, *19*, 409–418. [CrossRef]
36. Zhan, D.; Qiu, G.; Jiang, Z.; Zhang, H. Effect of Yttrium and Titanium on Inclusions and the Mechanical Properties of 9Cr RAFM Steel Fabricated by Vacuum Melting. *Steel Res. Int.* **2017**, *88*, 1700159. [CrossRef]
37. Gao, X.; Ren, H.; Wang, H.; Chen, S. Activity coefficient and solubility of yttrium in Fe-Y dilute solid solution. *J. Rare Earths* **2016**, *34*, 1168–1172. [CrossRef]
38. Ishii, F.; Ban-Ya, S. Equilibrium between yttrium and oxygen in liquid iron and nickel. *ISIJ Int.* **1995**, *35*, 280–285. [CrossRef]
39. Seo, W.; Han, W.; Kim, J.; Pak, J. Deoxidation equilibria among Mg, Al and O in liquid iron in the presence of $MgO{\cdot}Al_2O_3$ spinel. *ISIJ Int.* **2003**, *43*, 201–208. [CrossRef]

© 2019 by the authors. Licensee MDPI, Basel, Switzerland. This article is an open access article distributed under the terms and conditions of the Creative Commons Attribution (CC BY) license (http://creativecommons.org/licenses/by/4.0/).